Supporting Information for

Carbon Nanosheet Frameworks Derived from Peat Moss as High Performance Sodium Ion Battery Anodes

Jia Ding, [†,‡] *Huanlei Wang,* [†,‡] *Zhi Li,* [†,‡,*] *Alireza Kohandehghan,* [†,‡] *Kai Cui,* [‡] *Zhanwei Xu,* [†,‡] *Beniamin Zahiri,* [†,‡] *Xuehai Tan,* [†,‡] *Elmira Memarzadeh Lotfabad,* [†,‡] *Brian C. Olsen,* [†,‡] *and David Mitlin* [†,‡,*]

[†] Chemical and Materials Engineering, University of Alberta, Edmonton, Alberta T6G 2V4, Canada, [‡] National Institute for Nanotechnology (NINT), National Research Council of Canada, Edmonton, Alberta T6G 2M9, Canada

*****Address correspondence to lizhicn@gmail.com (Z. Li); dmitlin@ualberta.ca (D. Mitlin).

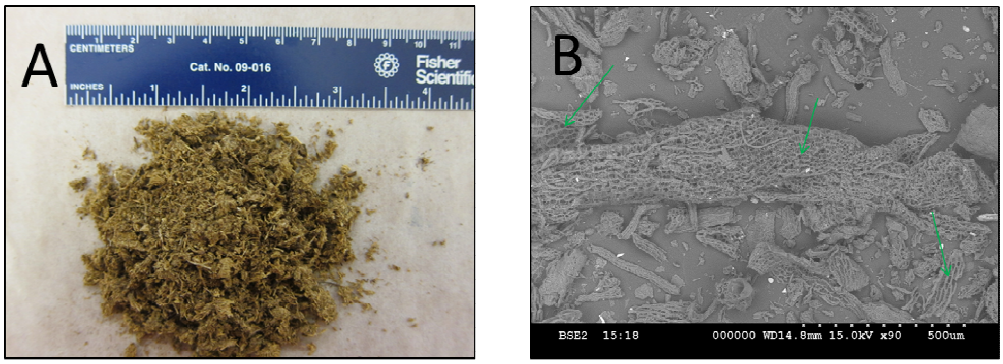

Figure S1. (A) Photograph of the fully dehydrated peat moss precursor. (B) Environmental SEM image of the dehydrated peat moss precursor.

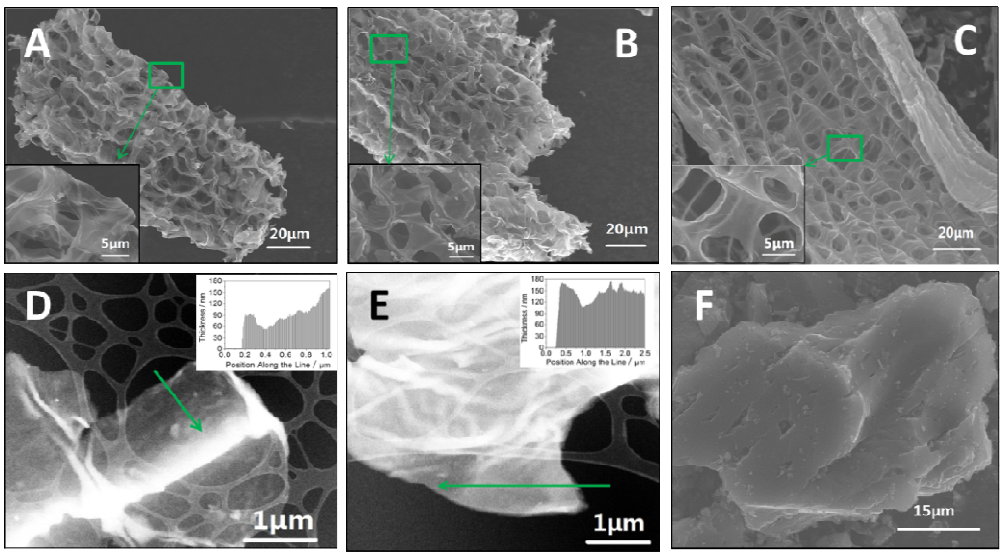

Figure S2. (A) SEM micrograph of an individual particle (CPM-900-A), highlighting the thin carbon films (inset). (B) SEM micrograph of CPM-1400-A. (C) SEM micrograph of CPM-1100-A, highlighting the macroporous architecture. (D-E) HAADF TEM micrographs and EELS thickness profile (insets) of carbon nanosheets in CPM-A. (F) SEM micrograph of a commercial activated carbon (CAC) particle.

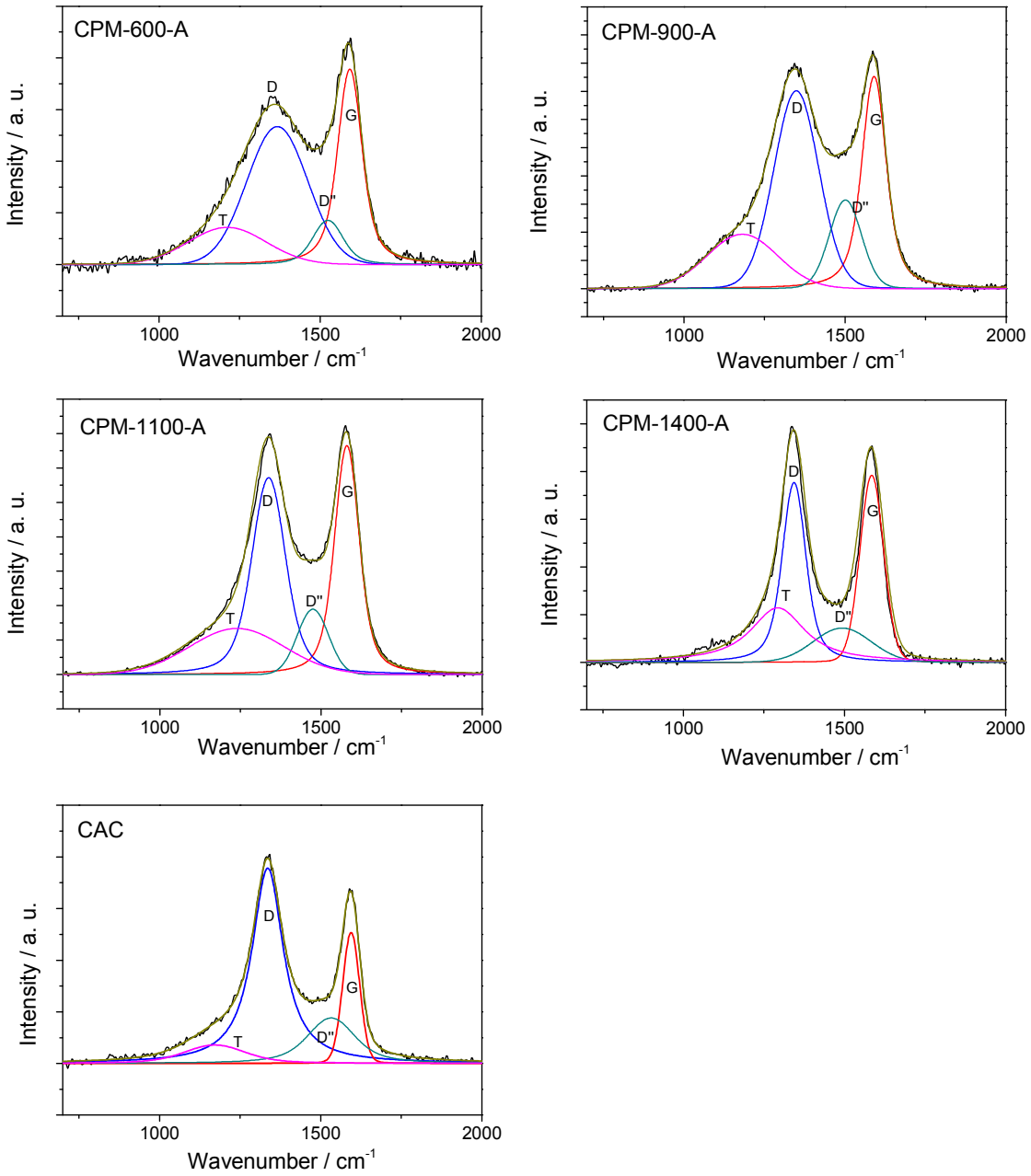

Figure S3. Fitted Raman spectra of CPM-A and CAC specimens.

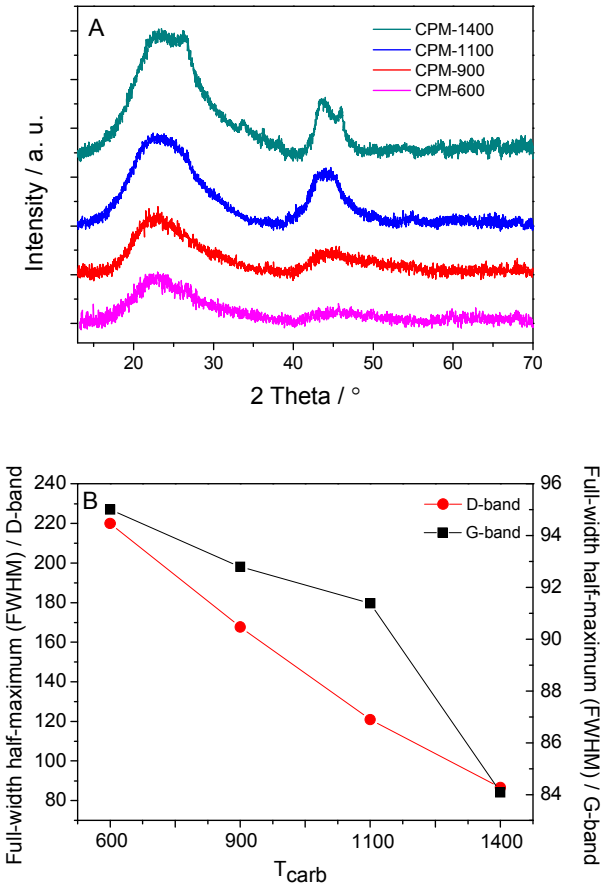

Figure S4. (A) XRD patterns of the un-activated specimens (CPM). (B) FWHM data of D-/ G-band as a function of carbonization temperature (CPM-A specimens).

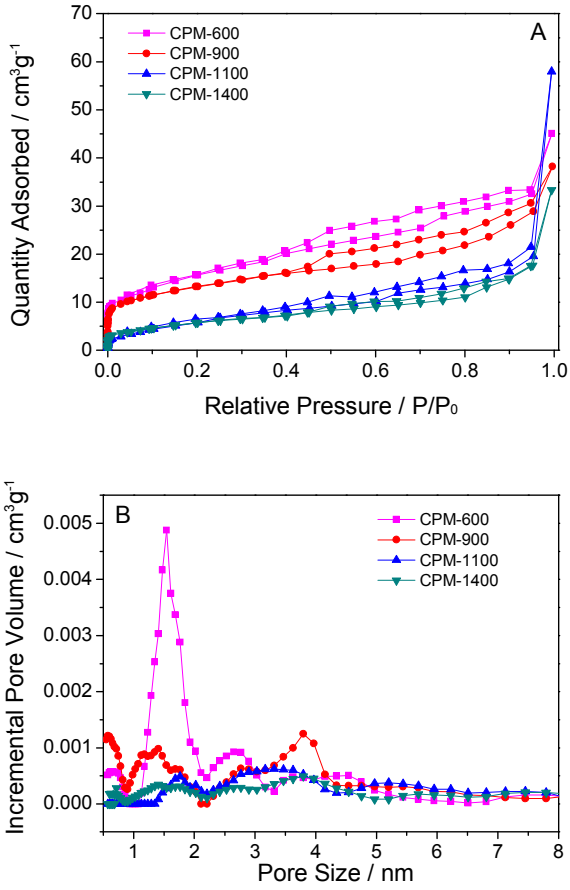

Figure S5. (A) Nitrogen adsorption-desorption isotherms of the CPM specimens. (B) Pore size distribution of CPM specimens, calculated from the adsorption isotherms using DFT method.

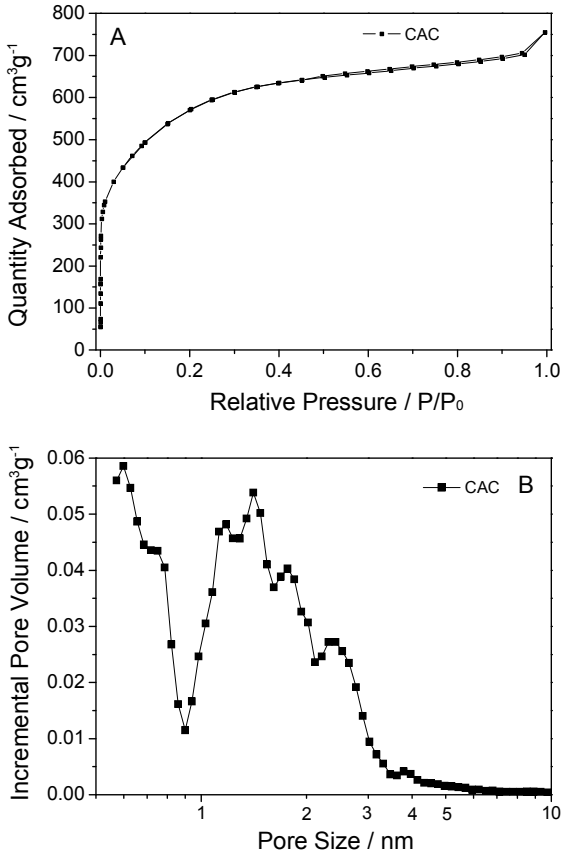

Figure S6. (A) Nitrogen adsorption-desorption isotherms of commercial activated carbon. (B) Pore size distribution of commercial activated carbon calculated from the adsorption isotherms using DFT method.

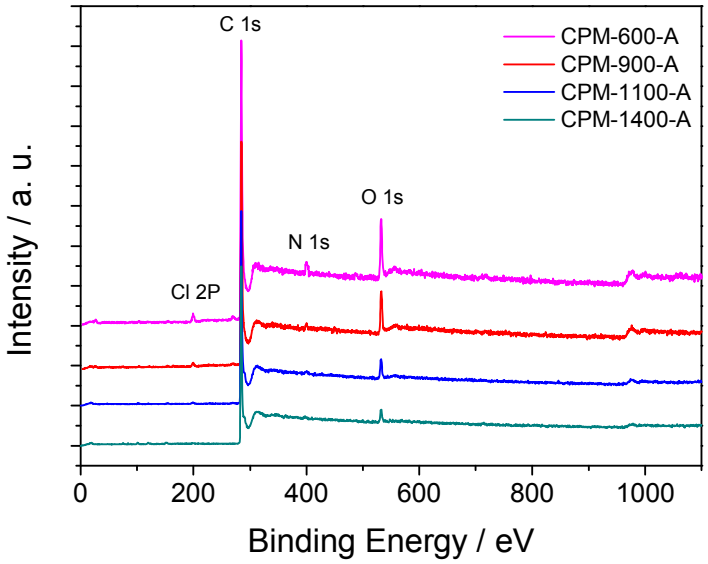

Figure S7. XPS survey spectra of CPM-A specimens. The minor amount of Cl came from the post-carbonization HCl acid wash.

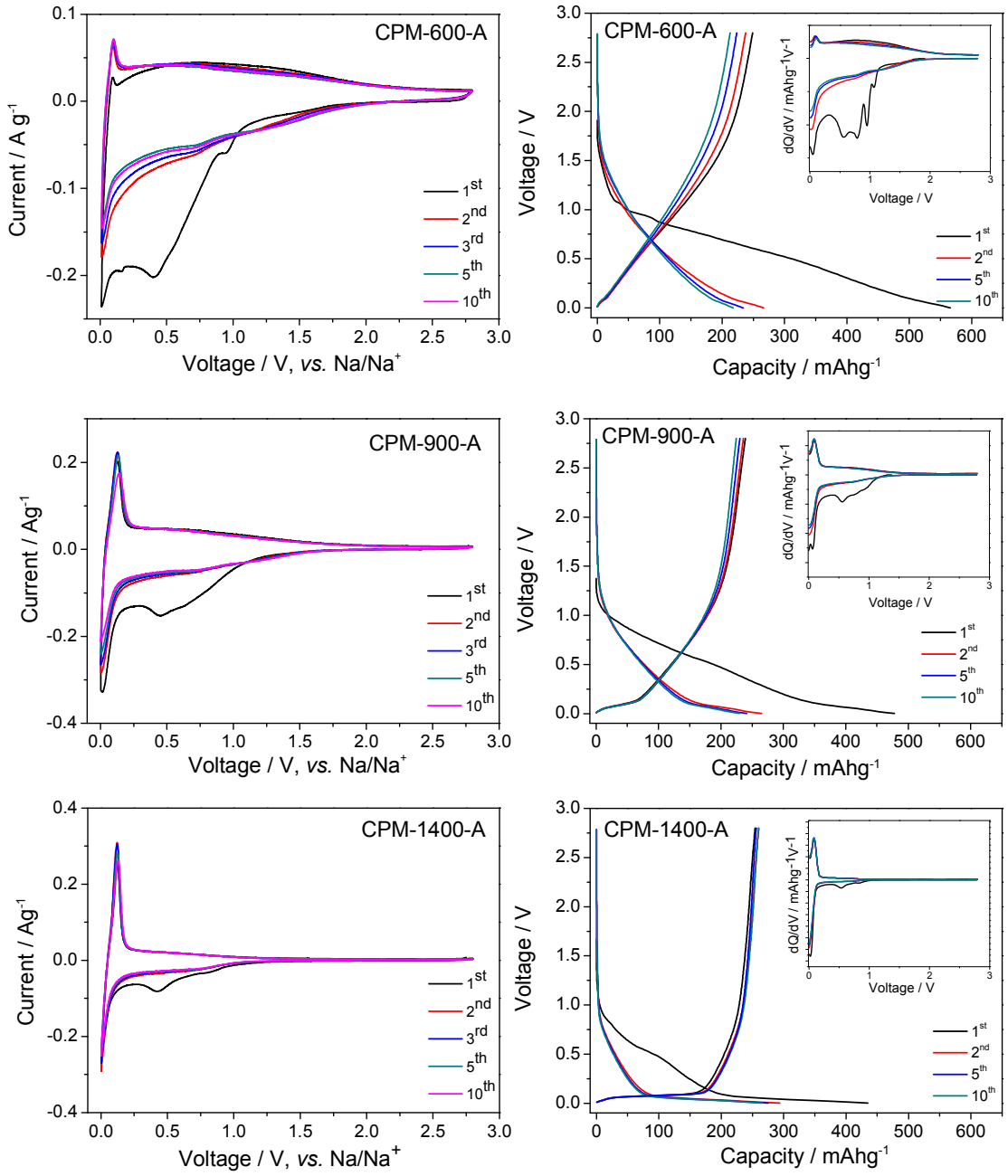

Figure S8. CV and galvanostatic discharge/charge profiles of CPM-A electrodes between 0.001 and 2.8 V at a scanning rate of 0.1 mVs^{-1}. Galvanostatic discharge/charge profiles are obtained at current density of $50mAg^{-1}$.

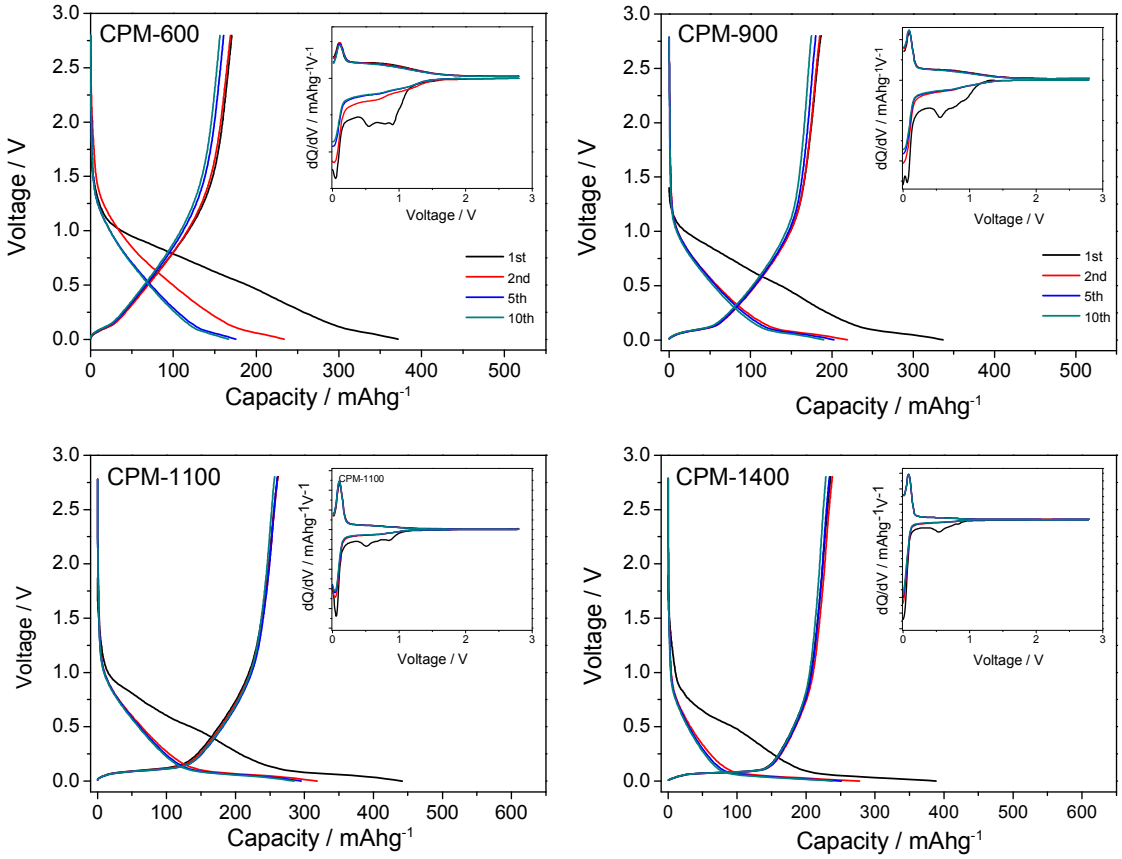

Figure S9. Galvanostatic discharge/charge profiles of un-activated CPM electrodes at a current density of 50mAg^{-1}.

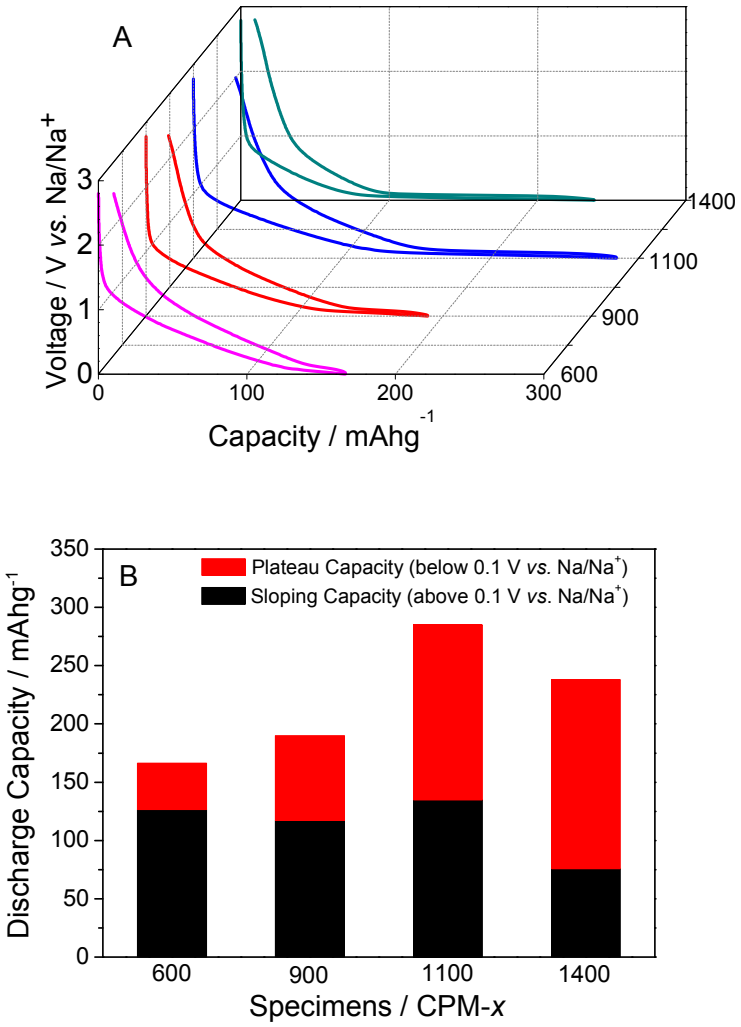

Figure S10. (A) Potential profiles of CPM electrodes. (B) Summary of capacity potential distribution of un-activated specimens (CPM). (10^{th} cycle at current density of $50mAhg^{-1}$ in both A and B).

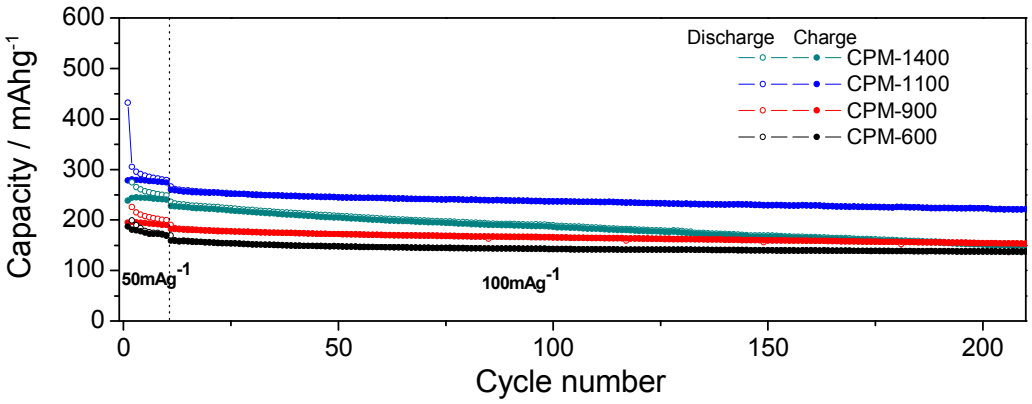

Figure S11. Extended cycling performance of CPM electrodes.

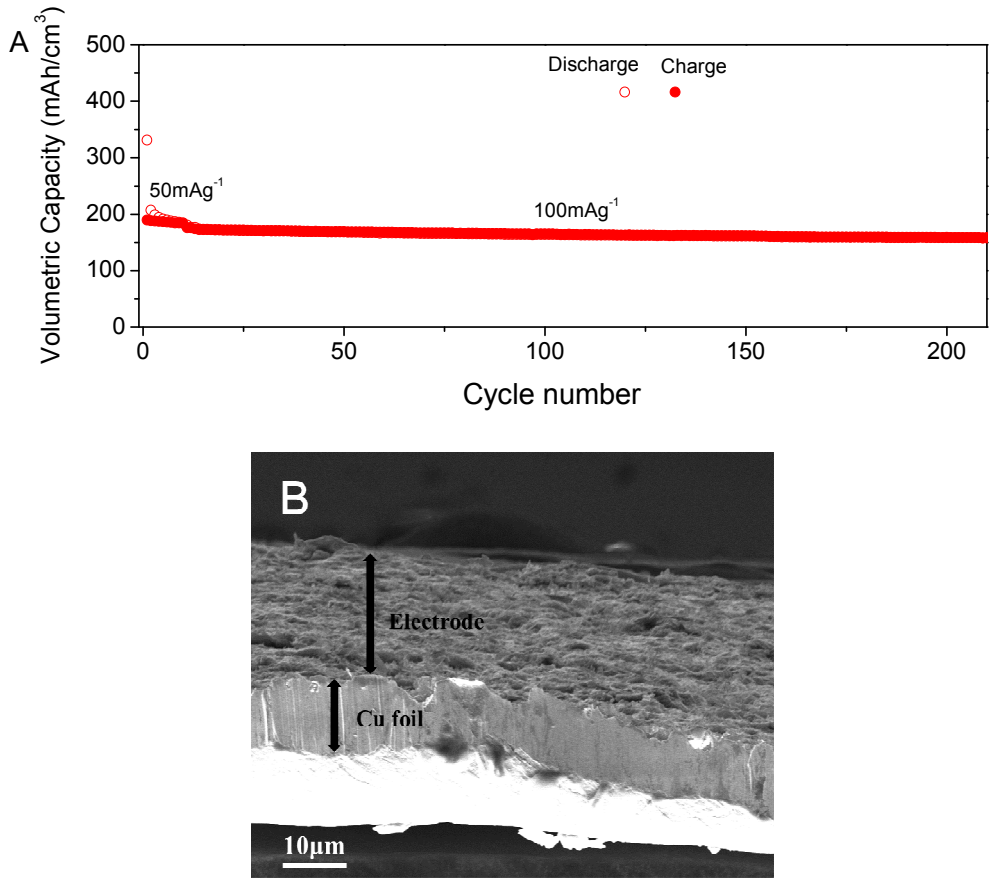

Figure S12. (A) Volumetric capacity of CPM-1100-A. (B) Cross section SEM image of the CPM-1100-A electrode.

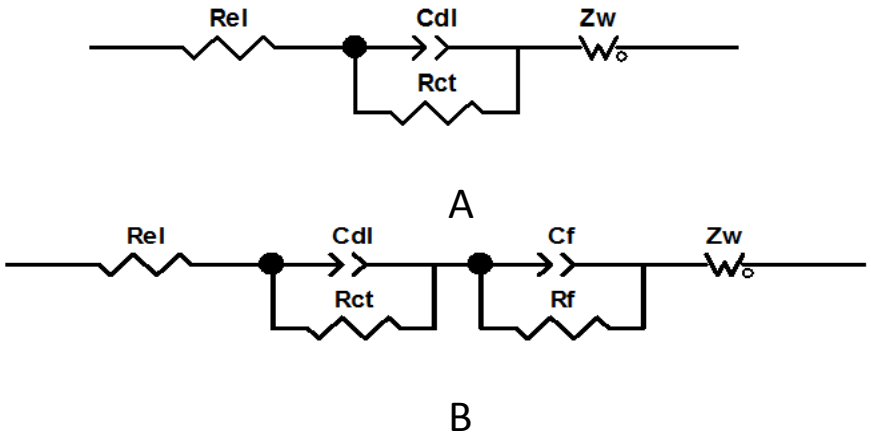

Figure S13. Equivalent electronic circuits used to simulate the EIS data. For the spectra of all the as prepared specimens, equivalent circuit (A) was used. R_{el} is the sum of resistances of electrical connections in the experiment setup including ionic diffusion resistance in the electrolyte. R_{ct} reflects the charge transfer resistance and Z_w (Warburg-type element) represents Na diffusion impedance within carbon materials.
For the cycled specimens with SEI layer formed (equivalent circuit B was used), another pair of resistor (R_f) and constant phase element (C_f) represent Na transport through SEI/carbon interface. R_{ct}+R_f is claimed to represent the total charge transfer resistance within all the interfaces and through SEI layer.

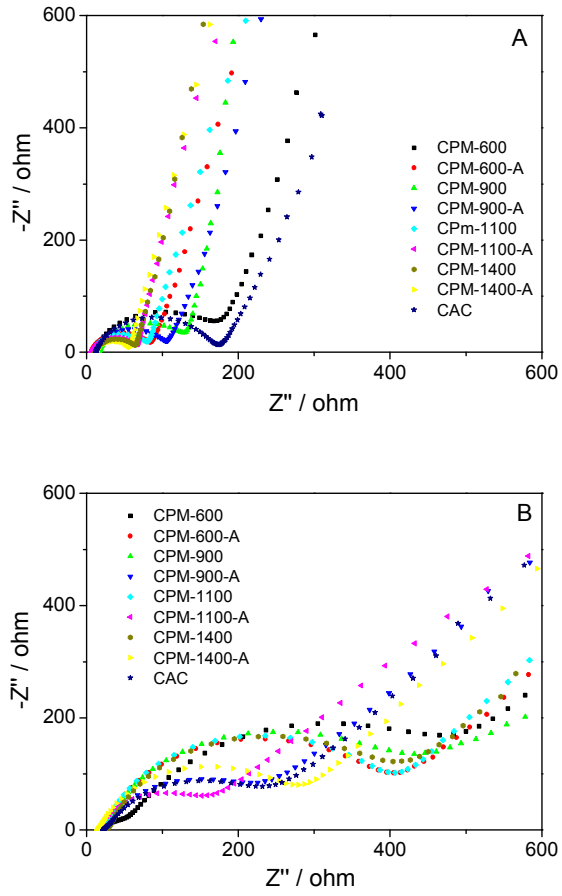

Figure S14. (A) Electrochemical impedance spectra of CPM, CPM-A and CAC electrodes before cycling. (B) Electrochemical impedance spectra of CPM, CPM-A and CAC electrodes after cycling for 210 cycles.

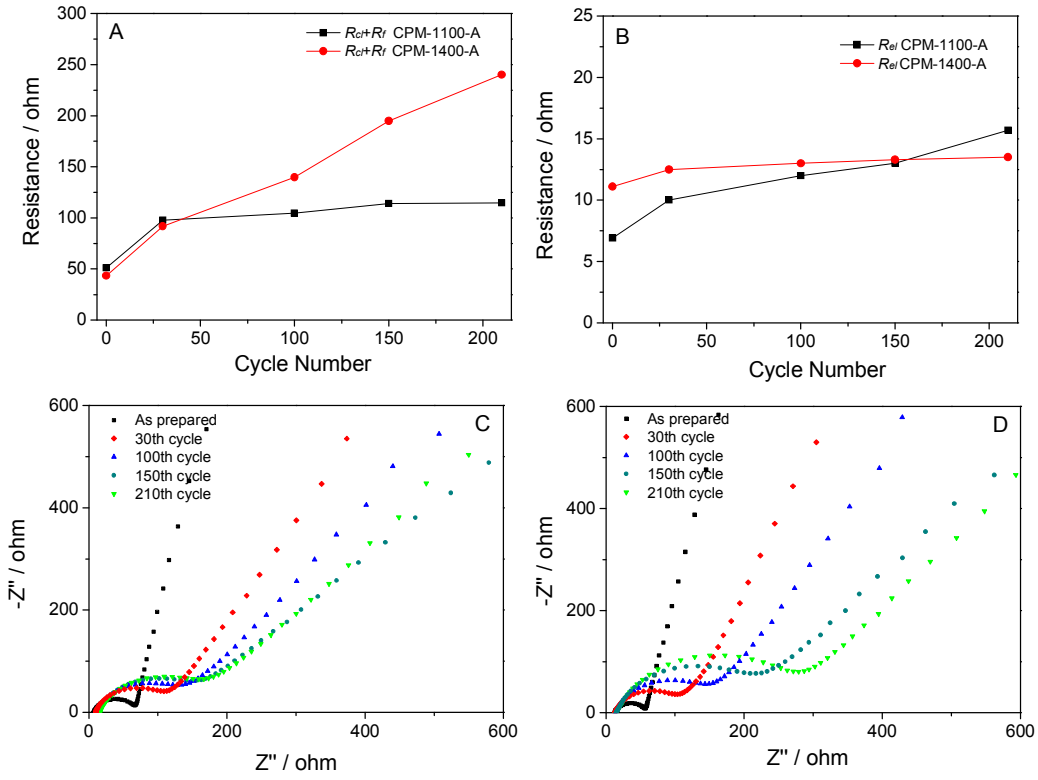

Figure S15. (A, B)The total charge transfer resistance within all the interfaces (R_{cl}+R_f) and sum of resistance of electrical connections in the experimental setup (R_{el}) changes as functions of the cycle number. (C, D) Electrochemical impedance spectra of CPM-1100-A (C) and CPM-1400-A (D) (As-prepared, 30th cycle, 100th cycle, 150th cycle and 210th cycle).

Table S1. Resistance values simulated from modeling the experimental impedance (Figure S14) using the equivalent circuits shown in Figure S13.

	CPM-600-A	CPM-900-A	CPM-1100-A	CPM-1400-A
As prepared electrodes				
R_{el} (Ω)	6.4	9.1	6.9	11.1
R_{ct} (Ω)	80.6	100.2	51.1	43.3
After cycled electrodes				
R_{el} (Ω)	15.2	23.8	15.7	13.5
R_{ct}+R_f (Ω)	324.5	182.7	114.7	240.1

	CPM-600	CPM-900	CPM-1100	CPM-1400
As prepared electrodes				
R_{el} (Ω)	9.3	16.1	8.5	11.2
R_{ct} (Ω)	172	119.7	72.1	52.6
After cycled electrodes				
R_{el} (Ω)	24.2	22.8	20.1	23.2
R_{ct}+R_f (Ω)	396	306.1	350.4	335.3

Table S2. Performance comparison of CPM-1100-A *versus* state of the art NIB carbons reported in literature

Material	Plateau capacity (capacity below 0.1 V *vs.* Na/Na^+)	Cyclability (discharge capacity)	Rate performance
Pyrolyzed glucose (Ref. 22)	150 $mAhg^{-1}$ (1^{st} cycle)	Not reported	Not reported
Carbon fibers (Ref. 23)	*ca*. 184 $mAhg^{-1}$ (1^{st} cycle)	Not reported	Not reported
Carbon microspheres (Ref. 24)	Not reported	285 $mAhg^{-1}$ at 2^{nd} cycle 255 $mAhg^{-1}$ at 7^{th} cycle 89% retention over 7 cycles at 40μAcm^{-2}	Not reported
Hard carbon particles (Ref. 25)	*ca*. 150 $mAhg^{-1}$ at 25mAg^{-1}	250 $mAhg^{-1}$ at 2^{nd} cycle 225$mAhg^{-1}$ at 100^{th} cycle 88% retention over 100 cycles at 25mAg^{-1}	Not reported
Templated carbon (Ref. 26)	*ca*. 20 $mAhg^{-1}$ at 74mAg^{-1} (10^{th} cycle)	180 $mAhg^{-1}$ at 10^{th} cycle, 120$mAhg^{-1}$ at 40^{th} cycle 66.7% retention over 30 cycles at 74mAg^{-1}	*ca*.140$mAhg^{-1}$ at 74mAg^{-1} *ca*.120$mAhg^{-1}$ at 740mAg^{-1} *ca*. 100$mAhg^{-1}$ at 1.85 Ag^{-1}
Hollow carbon spheres (Ref. 27)	*ca*. 20 $mAhg^{-1}$ at 50 mAg^{-1} (10^{th} cycle)	250 $mAhg^{-1}$ at 10^{th} cycle, 160 $mAhg^{-1}$ at 100^{th} cycle 64% retention over 90 cycles at 100mAg^{-1}	175$mAhg^{-1}$ at 200mAg^{-1} 150$mAhg^{-1}$ at 500mAg^{-1} 100$mAhg^{-1}$ at 2Ag^{-1} 75$mAhg^{-1}$ at 5Ag^{-1}
Hollow carbon nanowires (Ref. 29)	*ca*. 150 $mAhg^{-1}$ at 50mAg^{-1} (10^{th} cycle)	*ca*. 255 $mAhg^{-1}$ at 10^{th} cycle *ca*. 220 $mAhg^{-1}$ at 200^{th} cycle 86% retention over 190 cycles at 50 mAg^{-1}	*ca*. 210$mAhg^{-1}$ at 250mAg^{-1} 149 $mAhg^{-1}$ at 500mAg^{-1}
Carbon nanosheet (Ref. 28)	*ca*. 40 $mAhg^{-1}$ at 50mAg^{-1} (10^{th} cycle)	*ca*. 260$mAhg^{-1}$ at 10^{th} cycle *ca*. 155 $mAhg^{-1}$ at 200^{th} cycle 60% retention over 190 cycles at 50mAg^{-1}	*ca*. 190$mAhg^{-1}$ at 200mAg^{-1} *ca*. 125$mAhg^{-1}$ at 500mAg^{-1} *ca*. 80 $mAhg^{-1}$ at 1Ag^{-1} 50 $mAhg^{-1}$ at 2Ag^{-1} 45 $mAhg^{-1}$ at 5Ag^{-1}
CPM-1100-A (this work)	161 $mAhg^{-1}$ at 50 mAg^{-1} (10^{th} cycle)	284 $mAhg^{-1}$ at 10^{th} cycle 255$mAhg^{-1}$ at 210^{th} cycle 90% retention over 200 cycles at 100mAg^{-1}	250 $mAhg^{-1}$ at 200mAg^{-1} 203 $mAhg^{-1}$ at 500mAg^{-1} 150 $mAhg^{-1}$ at 1Ag^{-1} 106 $mAhg^{-1}$ at 2Ag^{-1} 66 $mAhg^{-1}$ at 5Ag^{-1}